THE JOURNAL OF PHYSICAL CHEMISTRY C

Article

Cite This: J. Phys. Chem. C 2019, 123, 14490−14500

pubs.acs.org/JPCC

# Preactive Site in Ziegler−Natta Catalysts

E. S. (Merijn) Blaakmeer, Frank J. Wensink, Ernst R. H. van Eck, Gilles A. de Wijs, and Arno P. M. Kentgens*

Institute for Molecules and Materials, Radboud University, Heyendaalseweg 135, 6525 AJ Nijmegen, The Netherlands

Supporting Information

**ABSTRACT:** Ziegler−Natta catalysts are one of the most important industrial catalysts for the production of isotactic polypropylene, yet they are still not properly understood at the molecular level. We explore the potential of $^{35,37}$Cl and $^{47,49}$Ti solid-state NMR to study the formation of catalytically relevant titanium sites. First, a systematic study of titanium chlorides ($TiCl_2$, $TiCl_3$, and $TiCl_4$) is undertaken to gain insight into the spectral characteristics for different titanium coordinations. For these materials, chlorine spectra can be relatively straightforwardly obtained, despite their strongly broadened quadrupolar line shapes. The sensitivity of titanium NMR to its local environment is exemplified by the $TiCl_4$ spectrum, for which a small quadrupolar interaction is found despite the nearly symmetric Ti coordination. Upon wet impregnation of $MgCl_2$ with $TiCl_4$, $TiCl_4$ is immobilized at the surface, retaining its tetrahedral coordination. For a ball-milled binary $MgCl_2/TiCl_2$ adduct, a ternary system where donors are added, and a ternary system where Al-alkyl cocatalysts are added, we obtain broad $^{47,49}$Ti spectra after extensive signal averaging, showing that the local environment of Ti is substantially perturbed. The span of the signal is similar for all three samples, suggesting that most of the donor and the cocatalyst do not directly bind to the titanium. Nevertheless, the signal loss from reduction to $Ti^{3+}$ is obvious, indicating that a fraction of the titanium sites is activated.

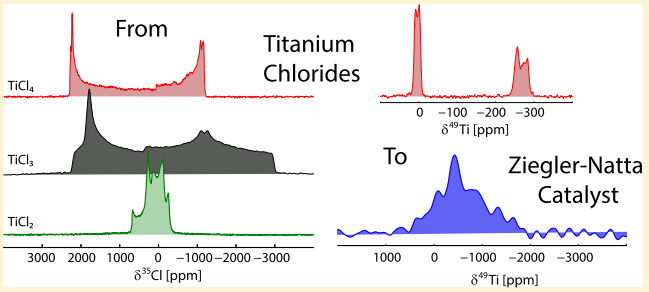




## INTRODUCTION

Ziegler−Natta catalysts (ZNCs) have been in use for decades with resounding successes, yet the fundamental understanding of their inner workings is limited; particularly, the nature of the active site still holds many secrets. In fact, there may well be multiple active sites, in contrast to homogeneous metallocene catalysts, which generally have a single active site, generating polymers with a narrow molecular weight distribution (MWD). $MgCl_2$-supported catalysts yield polymers with a much broader MWD, which is beneficial for their processability.[1] This broad MWD most likely results from the presence of multiple active sites, each generating polymers with a specific molecular weight (distribution).

The active sites are generated by the activation of $MgCl_2$-supported $TiCl_4$. Investigating the coordination of Ti in $TiCl_4$ and its interactions with the support is the first important step to shed light on the elusive active ZN site(s). There is consensus that the basal (001) surface, corresponding to a plane of chlorine atoms, cannot adsorb $TiCl_4$.[2] Recent literature suggests that binding of $TiCl_4$ monomers to the (110)-surface, the so-called Corradini site, is the preferential mode,[3−5] but little experimental evidence is around to support this claim.[5,6] Alternatively, $TiCl_4$ might bind to crystal defects that locally resemble the (110)-surface. Recent theoretical work postulates the existence of multinuclear binding involving the (104) surface or defects.[7]

NMR probes the local surroundings of the nuclei and can thus shed light on the fate of Ti on $MgCl_2$. Indeed, Ohashi et al.[8] demonstrated that solid-state NMR might be exploited to investigate the structure(s) of $TiCl_4$ in ball-milled adducts of $MgCl_2$ and $TiCl_4$. The potential of $^{47,49}$Ti NMR for heterogeneous catalysis was demonstrated by Rossini et al.[9] who reported the investigation of solid titanocene chlorides as models for metallocene catalysts. Their work included density functional theory (DFT) calculations and showed the strong influence of the coordinating ligands on the titanium nucleus, although the work also indicated some problems when dealing with real catalysts.

The successful acquisition of spectra of $TiCl_4$ would give the most direct handle on the active site formation. However, there are many challenges that have to be solved to achieve this ambitious aim: $^{47}$Ti and $^{49}$Ti are low abundance, low-$\gamma$ nuclei, which combined with strong quadrupolar line broadening, can impose sensitivity problems. Therefore, high external magnetic field strengths and signal enhancement schemes are a prerequisite. Moreover, besides the low gyromagnetic ratios, low natural abundance, and quadrupolar broadening, titanium NMR may also suffer from spectral overlap of the $^{47}$Ti and $^{49}$Ti resonances. Because of the small difference in gyromagnetic

Received: March 19, 2019
Revised: May 6, 2019
Published: May 15, 2019




DOI: 10.1021/acs.jpcc.9b02617
J. Phys. Chem. C 2019, 123, 14490−14500

ratio, the difference between the $^{49}$Ti and $^{47}$Ti resonances is only 267 ppm. On the 20.0 T magnet used for our experiments, this amounts to a difference of 12.8 kHz, so that both isotopes are generally detected simultaneously. In systems with strong quadrupolar interactions, this will lead to the overlap of the titanium resonances complicating the spectral analysis. Therefore, we first explore the ability of NMR to provide insight in the local coordination of Ti in relevant catalyst systems, that is, a systematic $^{35,37}$Cl and $^{47,49}$Ti solid-state NMR and DFT study of the titanium chlorides $TiCl_2$, $TiCl_3$, and $TiCl_4$ is performed. Subsequently, we move away from model systems and look at wet-impregnated $MgCl_2$ samples followed by ball-milled binary and ternary systems and finally an industrial precatalyst.

## EXPERIMENTAL SECTION

**Sample Preparation.** Titanium chlorides have been used as received from their suppliers: $TiCl_4$ (Honeywell), $TiCl_3$ (Sigma-Aldrich), and $TiCl_2$ (Sigma-Aldrich). For $MgCl_2/TiCl_4$ adducts, calcined (dried) $MgCl_2$ ($MgCl_2$ DC[10]) was used. Detailed sample preparations can be found in the Supporting Information. The industrial precatalyst CAT4 has been supplied by SABIC, and the ternary system TMC-M has been prepared as described elsewhere.[11] Rotors were filled under inert nitrogen atmosphere inside a glovebox.

**NMR Spectroscopy.** $^{35,37}$Cl and $^{47,49}$Ti spectra were recorded on a Varian VNMRS 850 MHz spectrometer (20.0 T, 83.3 MHz for $^{35}$Cl, 69.3 MHz for $^{37}$Cl, and 47.9 MHz for $^{47,49}$Ti) using triple resonance 1.6 and 4.0 mm Varian T3 MAS probes, a Varian VNMRS 600 MHz spectrometer (14.1 T, 48.9 MHz for $^{37}$Cl) using a triple resonance 1.6 mm Varian T3 MAS probe, and a Varian VNMRS 400 MHz spectrometer (9.4 T, 22.5 MHz for $^{47,49}$Ti) using a static goniometer probe custom tuned to the low frequency. The QCPMG pulse sequence[12] was used for most of the experiments. Transfer time of rotors to the magnet was kept to the minimum. Samples were constantly purged with a flow of dry nitrogen and, where applicable, spun using dry nitrogen gas. Cl and Ti shifts are referenced to aqueous solutions of NaCl or neat $TiCl_4$ (set to 0.0 ppm), respectively.

**Computational Details.** Calculations were carried out with the Vienna Ab initio Simulation Package (VASP)[13,14] using DFT and the projector augmented-wave (PAW) method.[15,16] We used both the PBE[17,18] and the hybrid HSE06[19] functional. The latter was needed because PBE fails to produce a gap for $TiCl_2$ and, for some orderings of the Ti magnetic moments, also for $TiCl_3$. Experimental crystal structures were used without further relaxation.[20−23] For the $MgCl_2$ slab models with $TiCl_2$ at the edges, however, we had to relax the structure (for details see Section S6 of the Supporting Information). NMR chemical shieldings were calculated with the gauge-including PAW method of refs[24,25] as implemented in VASP[26] and using PBE. Electric field gradients (EFGs) were calculated using the method of ref 27.

The Γ-centered $k$-point meshes were 2 × 3 × 2, 3 × 3 × 1, and 6 × 6 × 2 for $TiCl_4$, $TiCl_3$ (hexagonal cell), and $TiCl_2$, respectively. We used PAW potential files (unscreened using PBE) as supplied with VASP. Both the Ti (Ti_sv) and the Cl (Cl_h) potential had a frozen $1s^2 2s^2 2p^6$ core. The Mg (Mg_pv) had a frozen $1s^2$ core. For all calculations, we used the default kinetic energy cutoff for the Cl potential (Cl_h) of 409 eV. We checked convergence of $k$-points and cutoff. The nonlocal projections were carried out in real space.[28]

## RESULTS AND DISCUSSION

Studying titanium chlorides will provide insight into the typical NMR parameters that can be used for interpreting the results for supported titanium sites on $MgCl_2$. The active sites ultimately derive from $TiCl_4$, so it makes sense to start our investigations with this compound. At room temperature, it is a liquid, however. Also, the titanium coordination in $TiCl_4$ is different from the proposed model for supported $TiCl_4$. In the coordination mode of $TiCl_4$ on the (110)-surface of $MgCl_2$, the so-called Corradini site, titanium forms two additional bonds with surface chlorines, resulting in a hexacoordinated titanium site. Such a hexacoordination is found in $TiCl_2$ and $TiCl_3$, where titanium is octahedrally coordinated by six chloride ligands. These compounds might therefore give more relevant spectra for the interpretation of the spectra of supported $TiCl_4$.

**$TiCl_4$.** *Liquid $TiCl_4$.* Titanium tetrachloride is used as the titanium source in modern day ZNCs. The colorless, volatile liquid reacts violently with water to form titanium oxide and hydrogen chloride and should therefore be handled with care. The $^{47,49}$Ti NMR spectrum is shown in Figure S1A. As expected, two signals are obtained, one from each respective titanium isotope. Because of the high mobility in the liquid state, very sharp signals are observed and the lines for both isotopes are nicely separated. The $^{35}$Cl spectrum for liquid $TiCl_4$ can readily be obtained as well (see Figure S1B). The $^{35}$Cl resonance is found at a high isotropic chemical shift of 865 (±5) ppm. This value is still within the chlorine chemical shift range,[29] as perchlorates resonate around 1040 ppm,[30] but it is significantly higher than $MgCl_2$ (131 ppm) or group IV organometallic chlorides such as $Cp_2TiCl_2$ (∼500 ppm).[31]

*Solid $TiCl_4$.* The $^{47,49}$Ti spectrum of liquid $TiCl_4$, with its narrow lines, cannot be expected to give much insight into the titanium NMR of ZNCs. Solid-state NMR experiments of $TiCl_4$ are possible below the melting point of −24 °C. Although the titanium atom is tetrahedrally coordinated by four chlorine atoms, the tetrahedron is not perfectly symmetric. As a matter of fact, the chlorine sites in the crystal lattice are all inequivalent and the Ti−Cl bond distances and Cl−Ti−Cl bond angles vary slightly. This has implications for the EFG at the titanium site; hence, it affects the quadrupolar interaction parameters. The numbers in Table 1, obtained from DFT calculations using the HSE06 functional, indeed indicate that the $TiCl_4$ tetrahedra are not perfectly symmetric. A small $C_Q$ of 1.24/1.51 MHz is found for $^{49}$Ti/$^{47}$Ti, whereas it should be zero for an isolated perfect tetrahedron.

Because they are inequivalent, the four chlorine atoms all have slightly different $C_Q$ and $\eta_Q$ values, although they turn out to be very similar. These calculations are in line with $^{35}$Cl quadrupolar frequencies, $\omega_Q$, reported on the basis of nuclear quadrupolar resonance (NQR) experiments that report three or four $\omega_Q$ frequencies of around 6 MHz (corresponding to a $C_Q$ value of ∼12 MHz).[32−34]

Indeed, substantial quadrupolar broadening is observed in the $^{35}$Cl spectrum of solid $TiCl_4$ (Figure 1). The spectrum is obtained using a variable offset approach,[35,36] taking 10 Hahn echo spectra at intervals of 30 kHz. Although the spectrum spans 3500 ppm or 300 kHz, it still shows a well-defined powder pattern, with sharp peaks at the edges of the spectrum and a step around 0 ppm. As indicated by the DFT calculations, four $^{35}$Cl subspectra can be expected because of the nonequivalence of the four chlorines. The presence of



DOI: 10.1021/acs.jpcc.9b02617
J. Phys. Chem. C 2019, 123, 14490−14500

**Table 1. Quadrupolar Parameters (Absolute Values) Resulting from Our Experiments and DFT Calculations (HSE06 Functional) Based on the Crystal Structures for Solid $TiCl_4$[20] and $TiCl_3$[21]**

| atom | $C_Q$ [MHz] | $\eta_Q$ |
|---|---|---|
| | **$TiCl_4$** | |
| $^{35}$Cl (exp.) | 12.0 ± 0.1 | 0 ± 0.03 |
| $^{35}$Cl−1 | 12.43 | 0.02 |
| $^{35}$Cl−2 | 12.44 | 0.03 |
| $^{35}$Cl−3 | 12.49 | 0.04 |
| $^{35}$Cl−4 | 12.64 | 0.02 |
| $^{47}$Ti (exp.) | 1.38 ± 0.05 | 0.6 ± 0.1 |
| $^{47}$Ti | 1.51 | 0.61 |
| $^{49}$Ti | 1.24 | 0.61 |
| | **$TiCl_3$** | |
| $^{35}$Cl (exp.) | 14.5 ± 0.1 | 0.4 ± 0.04 |
| $^{35}$Cl AF[a] | 14.67 | 0.24 |
| $^{35}$Cl FM[a] | 14.67 | 0.24 |
| $^{47}$Ti (exp.) | | |
| $^{47}$Ti AF[a] | 57.07 | 0 |
| $^{47}$Ti FM[a] | 56.92 | 0 |

[a]Both an AF and FM magnetic structure where considered. For AF, a structure with all nearest neighbor Ti moments antiparallel was used.

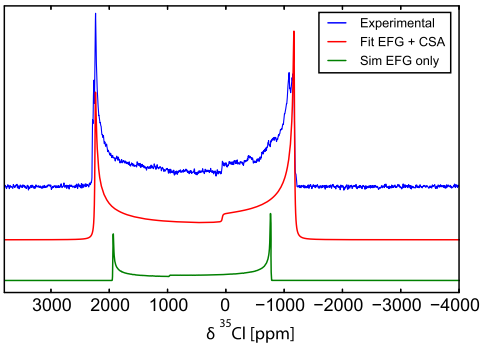


**Figure 1.** Static $^{35}$Cl NMR Hahn echo spectrum (skyline projection) of frozen $TiCl_4$ (−30 °C) obtained using the VOCS approach taken 10 spectra at 30 kHz intervals with 1024 scans each.

subspectra with slightly different quadrupolar parameters is indeed detected in the fine structure on the peaks at both edges of the spectrum (see Figure S3).

Irrespective of this fine structure, the overall line shape is not in agreement with a simple second-order quadrupolar powder pattern as is clear from a comparison to the simulation shown in green. This simulation is performed for a single site with $C_Q$ = 12 MHz and $\eta$ = 0. Simply increasing $C_Q$ to a value of ∼13.5 MHz will give a broader line and hence a better fit, but it cannot correctly describe the line shape. The discontinuity in the experimental spectrum is shifted significantly to the right compared to a second-order quadrupolar powder pattern.

We obtained a good description of the experimental line shape by including chemical shift anisotropy (CSA). To this end, the spectrum was fitted using SIMPSON,[37] giving the red trace in Figure 1. For robustness, we fitted the whole spectrum with a single site that will give an average $C_Q$ of the four chlorine sites. The resulting fitting parameters are: $C_Q$ = 12.0 (±0.1) MHz, $\eta_Q$ = 0 (±0.03), $\delta_{iso}$ = 875 (±5) ppm, $\delta_{aniso}$ = −805 (±10) ppm, and $\eta_{CSA}$ = 0 (±0.03). A good agreement of the experimental span is reached, whereas the $C_Q$, at the same time, is in agreement with the literature. The position of the discontinuity also matches nicely. The isotropic chemical shift in the solid state is almost the same as in the liquid state. The small difference in shift can actually be explained by the difference in temperature in the experiments. Large chlorine CSAs have been reported before for metallocenes,[31] and smaller, but still detectable, anisotropies were found for alkaline earth chlorides[38] and hydrochloride salts of amino acids.[39,40] On the basis of the close to tetrahedral symmetry, an $\eta_{CSA}$ close to zero is to be expected. With $\eta$ = 0 for both the quadrupolar interaction and the CSA, only one angle ($\beta$) is required to relate the two interaction frames with respect to each other. We obtain $\beta$ = 0° with the fit being very sensitive to small deviations from this angle, so the tensors of the quadrupolar and CSA are co-aligned.

DFT calculations were performed to calculate the chlorine chemical shift (Table S1) for which we needed to use a different functional (PBE). These calculations gave slightly different quadrupolar parameters compared to those calculated using the HSE06 functional. However, these EFG parameters are still in agreement with experimental values. Also, both functionals yielded a band gap (in contrast to $TiCl_2$, vide infra). The average CSA parameters ($\delta_{aniso}$ = −805 ppm, $\eta_{CSA}$ = 0.01) are in excellent agreement with experimental values.

Similar to liquid $TiCl_4$, the $^{47,49}$Ti spectrum of frozen $TiCl_4$, shown in Figure 2, displays two resonances: one for $^{49}$Ti and

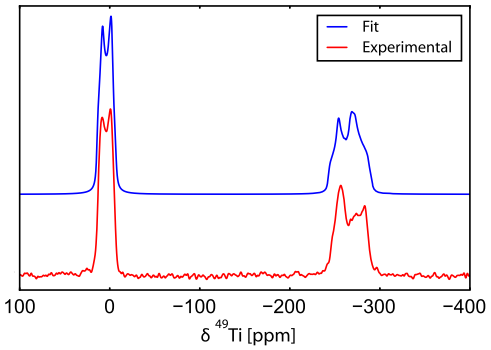


**Figure 2.** Static $^{47,49}$Ti NMR spectrum of frozen $TiCl_4$ (red) obtained by single pulse excitation. The results from a simultaneous fit of the $^{47}$Ti and $^{49}$Ti resonance, taking into account quadrupolar interaction and CSA, are shown in blue.

one for $^{47}$Ti. The resonances are significantly broader compared to the spectrum of the liquid, however. The $^{47}$Ti signal is clearly broader than the $^{49}$Ti signal, and both resonances show some characteristic quadrupolar features, as was already indicated by the DFT calculations. The difference in line width between the $^{49}$Ti and $^{47}$Ti resonance has two reasons. The combined effects of the different quadrupole moment and spin quantum number of the isotopes result in a $^{47}$Ti central transition (CT) line width that is ∼3.5 times larger than the $^{49}$Ti CT line width. The ratio of the experimental line widths observed in Figure 2 is, however, somewhat smaller than this.

The quadrupolar parameters can be obtained by simultaneous fitting of the $^{47}$Ti and $^{49}$Ti resonances using the ssNake software package[41] (see Figure S2). Fitting results improve when both the quadrupolar interaction and the CSA are included in the fit. As can be seen in Figure 2, in particular, the line shape of the $^{49}$Ti resonances and the line widths of both



DOI: 10.1021/acs.jpcc.9b02617
J. Phys. Chem. C 2019, 123, 14490−14500

the $^{47}$Ti and $^{49}$Ti resonance match well. The resulting parameters are: $^{49}$Ti $C_Q$ = 1.13 (±0.05) MHz, $^{47}$Ti $C_Q$ = 1.38 (±0.05) MHz, $\eta_Q$ = 0.6 (±0.1), $\delta_{iso}$ = 5 (±1) ppm, $\delta_{aniso}$ = −6 (±1) ppm, and $\eta_{CSA}$ = 0.7 (±0.1), and the angles $\alpha$, $\beta$, and $\gamma$ are 30 ± 5°, 15 ± 5°, and 220 ± 5°, respectively. The calculated parameters, both for the EFG and for the shielding (Table S1), are in agreement with the experiment.

All in all, the calculated NMR parameters for $TiCl_4$, both for $^{35}$Cl and $^{47,49}$Ti, match the experimental ones quite well. A slight deviation from the symmetric tetrahedron was predicted to already give a sizeable quadrupolar interaction, which is indeed observed. This proves that $^{47,49}$Ti NMR provides information about the local symmetry at the titanium site.

**$TiCl_3$.** Titanium trichloride has four different crystal polymorphs known as $\alpha$-, $\beta$-, $\gamma$-, and $\delta$-$TiCl_3$,[42] in all of which titanium is octahedrally coordinated by chlorines. The X-ray diffraction (XRD) analysis indicates that our sample is the $\alpha$-polymorph that has a layered structure in which the chlorine atoms are hexagonal close-packed.[21] From the crystal structure, a single chlorine resonance in NMR experiments is expected, as all chlorines should be equivalent. Similarly, only a single Ti-resonance (per isotope) is expected. The $^{35}$Cl NMR QCPMG spectrum of $\alpha$-$TiCl_3$ is shown in Figure 3. The

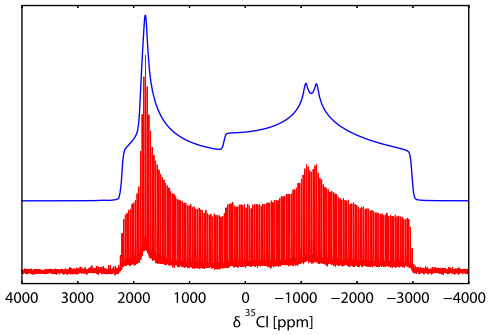


**Figure 3.** Static $^{35}$Cl QCPMG NMR spectrum of $\alpha$-$TiCl_3$ (red) obtained using the VOCS approach summing 15 subspectra at 40 kHz difference with 8192 scans each, $B_0$ = 20.0 T. Fit of the spectrum taking into account both quadrupolar interaction and CSA (blue).

spectrum displays well-defined features and spans >5000 ppm (430 kHz), indicating a strong quadrupolar interaction, as is predicted by DFT calculations (see Table 1). However, the quadrupolar interaction only cannot account for the observed line shape. Similarly to $TiCl_4$, it is necessary to include a CSA contribution to accurately fit the spectrum.

The spectrum was fitted using SIMPSON and, in agreement with the crystal structure, could be described by a single site with the following NMR parameters: $C_Q$ = 14.5 (±0.1) MHz, $\eta_Q$ = 0.4 (±0.03), $\delta_{iso}$ = 500 (±10) ppm, $\delta_{aniso}$ = 318 (±10) ppm, and $\eta_{CSA}$ = 0.72 (±0.1), and the angles $\alpha$, $\beta$, and $\gamma$ between the two tensors are 0 ± 1°, 90 ± 1°, and 30 ± 1°. The obtained quadrupolar parameters are in excellent agreement with the NQR frequency (7.39 MHz) reported by Barnes and Segel.[43]

Note that we could not reliably calculate the shielding parameters for $TiCl_3$ by DFT because the presence of the magnetic moment of $TiCl_3$ is not included in the protocol. Table 1 therefore only includes quadrupole parameters, calculated based on the reported crystal structure. For $TiCl_3$, the HSE06 functional appears much more realistic than the PBE functional. The latter yielded no or a small band gap of just a few tens of eV, depending on the ordering of the Ti magnetic moments. There is an excellent agreement with the experimental $C_Q$ value, and $\eta$ also matches quite well. We see little effect between structures with antiferromagnetic (AF) ordering of the magnetic structure with respect to the ferromagnetic (FM) ordering, for both chlorine and titanium.

The calculated $C_Q$ of 57 MHz for $^{47}$Ti is very large which would result in extremely broadened spectra with line widths in the MHz regime, even for $^{49}$Ti (0.6 ($\eta$ = 0) to 1.2 ($\eta$ = 1) MHz). Indeed, despite numerous attempts, no titanium spectrum could be obtained for $TiCl_3$. For $TiCl_2$ (vide infra), we were able to detect signal spanning hundreds of kHz and we would like to stress that the pulse sequences that did work for $TiCl_2$ gave no results for $TiCl_3$. Besides the very strong quadrupolar interaction, $TiCl_3$ also has unpaired electrons that usually cause extremely fast relaxation and further line broadening. It might be that paramagnetic effects contribute to the failure to acquire Ti signals for $TiCl_3$.

$TiCl_3$ has been reported to be a low-mobility semiconductor.[44] For conducting samples, one often encounters problems with spinning and efficient excitation is prevented by a low penetration depth of the RF field for such samples. Such problems where, however, not experienced by us, indicating that $TiCl_3$ is not a conductor. Nevertheless, it is remarkable that we do not observe paramagnetic effects in the $^{35}$Cl spectrum. Note that we also did not observe an EPR signal for $TiCl_3$ (at room temperature, X-band). Maurelli et al.[45] report on the presence of strong exchange interactions in solid $TiCl_3$ which lead to EPR-silent states. They report low-temperature (10 K) EPR spectra for $\alpha$- and $\beta$-$TiCl_3$, but explain the observed spectra as relating to defect structures in these materials.

**$TiCl_2$.** Titanium dichloride is a black solid that has not been studied intensively, most likely because of its high reactivity.[46] It reacts vigorously with water or oxygen as Ti(II) is a strong reducing agent. The reported crystal structure of $TiCl_2$ consists of layers of titanium atoms octahedrally coordinated by six equivalent chlorine atoms.[22,23]

The static $^{35}$Cl NMR spectrum of $TiCl_2$ is shown in Figure 4A. From this spectrum, it is immediately clear that there are multiple chlorine resonances. Even by the inclusion of CSA, this line shape cannot result from a single chlorine site. The spectrum is notably narrower than that for $TiCl_3$ and solid $TiCl_4$, but still spans ∼90 kHz. Figure 4B shows a 32 kHz wide spectrum under magic angle spinning (MAS) conditions. Because the second-order quadrupolar interaction is not completely averaged by MAS the resonances possess characteristic quadrupolar features, but the lines are narrowed. Therefore, the MAS spectrum yields enhanced resolution, and at least three distinct resonances can be distinguished, all relating to well-defined structural sites, indicating that the material is not strongly disordered or amorphous. However, despite the fast MAS, there is still an overlap between the CTs and spinning sidebands, as indicated by the asterisks in the figure.

To resolve this issue, we recorded a MAS ($\nu_r$ = 37 kHz) spectrum for $^{37}$Cl, as shown in Figure 4D. Because of a lower quadrupole moment, the $^{37}$Cl spectra are narrower so that the spinning sidebands can be clearly separated from the CTs. The static $^{37}$Cl NMR spectrum of $TiCl_2$ is also obtained and shown in Figure 4C. Its line shape and width are very comparable to the static $^{35}$Cl spectrum. The results from simultaneously fitting the $^{35}$Cl and $^{37}$Cl MAS spectra using ssNake[41] are


DOI: 10.1021/acs.jpcc.9b02617
J. Phys. Chem. C 2019, 123, 14490−14500

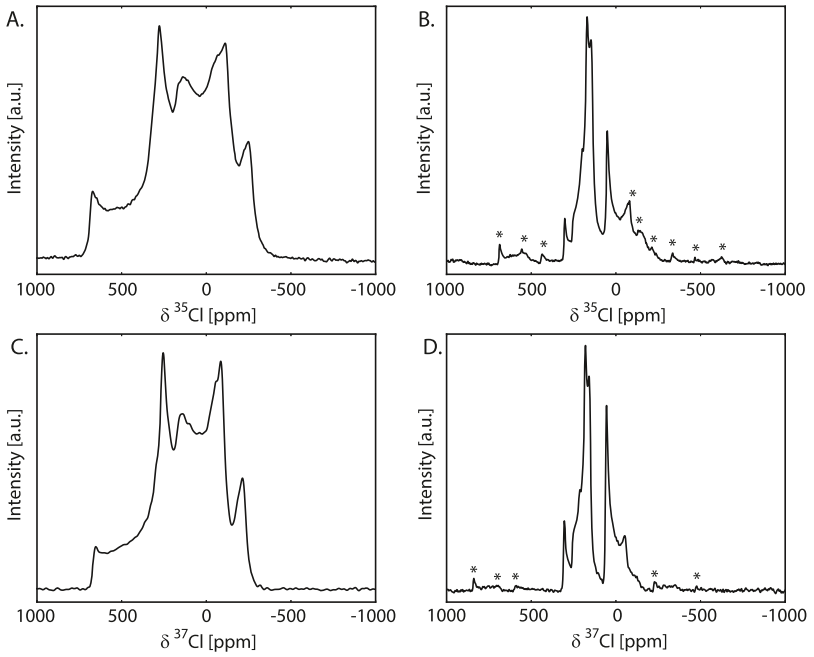


**Figure 4.** $^{35}$Cl Hahn echo (A,B) and $^{37}$Cl QCPMG (C,D) NMR spectra of $TiCl_2$ obtained under static (A,C) and MAS ((B) 32 to (D) 37 kHz) conditions, $B_0$ = 20.0 T. The static $^{35}$Cl spectrum is obtained using the VOCS approach taking 6 spectra at 40 kHz offset with 1024 scans each. Spectra (B–D) are acquired with 4096, 864, and 4096 scans, respectively. Asterisks denote features from spinning sidebands.

shown in Figure S4. We find three chlorine resonances and their corresponding NMR parameters are given in Table 2.

**Table 2. Results from Simultaneous Fitting of the $^{35}$Cl and $^{37}$Cl MAS Spectra of $TiCl_2$**

| $\delta_{iso}$ [ppm] | $C_Q$[a] [MHz] | $\eta_Q$ | rel. int |
|---|---|---|---|
| 336 (±2) | 4.97 (±0.1) | 0.04 (±0.05) | 0.07 (±0.02) |
| 257 (±2) | 4.62 (±0.1) | 0.79 (±0.05) | 0.62 (±0.02) |
| 94 (±2) | 5.51 (±0.1) | 0 (±0.05) | 0.31 (±0.02) |

[a] $C_Q$ are given for $^{35}$Cl.

Note that we could not satisfactorily fit the static spectra (Figure S5) which is attributed to CSA contributions to the resonances which cannot be reliably fitted because of the spectral overlap. We interpret the relative intensities of the resonances as follows: there are two main components, with a relative intensity of 2:1 and a minor component (at 335.7 ppm) that is most likely an impurity. It should be noted that the relative intensities of the peaks vary between the measurements. The given value is an average of the different fit results.

Overall, the $^{35}$Cl MAS spectra can be nicely fitted using multiple chlorine sites. This is puzzling because it does not correspond to the proposed crystal structure. Old data from NQR measurements suggest a single site, in agreement with the crystal structure.[43] The reported $^{35}$Cl $\omega_Q$ of 4.17 MHz corresponds to a significantly larger $C_Q$-value than found here. However, our powder XRD pattern is in good agreement with the literature (see Figure S6).

The titanium spectrum of $TiCl_2$, as shown in Figure 5, is extremely broad. The CT's of $^{47}$Ti and $^{49}$Ti together span a frequency range of >500 kHz. The signal above 450 kHz and below −200 kHz results most likely from satellite transitions (STs) and/or the CT of $^{47}$Ti. Interestingly, the broad spectrum is not featureless but shows two peaks at 50 and 250 kHz.

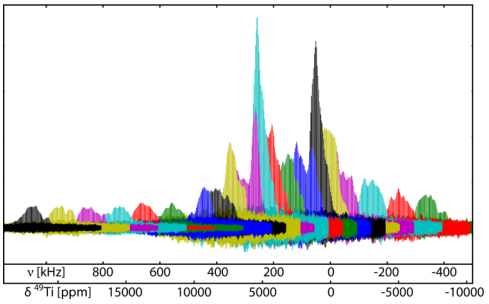


**Figure 5.** Static $^{47,49}$Ti NMR variable offset QCPMG spectra of $TiCl_2$, $B_0$ = 20.0 T.

Assuming this is due to the $^{49}$Ti CT, this would correspond to a $C_Q$ around 27 MHz [corresponding to a $C_Q \approx 33$ MHz and a CT line width of 700 kHz for $^{47}$Ti (assuming $\eta$ = 0)]. The titanium site in $TiCl_2$ is in the center of a fairly symmetric octahedron. In the case of $MgCl_2$, which has a very similar crystal structure,[47] the octahedra are also slightly distorted, giving a small quadrupolar interaction for $^{25}$Mg. For $TiCl_4$, with slightly distorted tetrahedra, small quadrupolar couplings were found as well. The $^{47,49}$Ti NMR spectrum of $TiCl_2$ indicates a much larger quadrupolar interaction and thus a much more sizeable EFG which must then be due to asymmetries in the higher coordination spheres of titanium in this structure.

Table 3 reports EFG parameters calculated for several published structures of $TiCl_2$. Again, we cannot include shielding parameters in the calculation (for the same reason as discussed above for $TiCl_3$). The HSE06 functional was needed because PBE predicts $TiCl_2$ to be metallic. As follows from the crystal symmetry, there should be only a single chlorine site in the crystal structures reported by Gal'perin and Baenziger. It is interesting to see that significantly smaller $^{35}$Cl $C_Q$ parameters are obtained compared to $TiCl_4$ and $TiCl_3$.



DOI: 10.1021/acs.jpcc.9b02617
J. Phys. Chem. C 2019, 123, 14490−14500

**Table 3. Quadrupolar Parameters (Absolute Values) Resulting from DFT Calculations (HSE06 Functional) Based on Varying Structures Solid $TiCl_2$**

| atom | $C_Q$ [MHz] | $\eta_Q$ | structure |
|---|---|---|---|
| $^{35}$Cl FM | 5.32 | 0.00 | Gal'perin[22] |
| $^{35}$Cl FM | 5.38 | 0.00 | Gal'perin[22] "$\alpha$-$MgCl_2$ stacking" |
| $^{35}$Cl AF | 5.21 | 0.15 | Gal'perin[22] |
| $^{35}$Cl FM | 1.88 | 0.00 | Baenziger[23] |
| $^{35}$Cl FM | 1.56 | 0.00 | Vlaic[48a] |
| $^{47}$Ti FM | 30.25 | 0.00 | Gal'perin[22] |
| $^{47}$Ti FM | 30.23 | 0.00 | Gal'perin[22] "$\alpha$-$MgCl_2$ stacking" |
| $^{47}$Ti AF | 27.84 | 0.78 | Gal'perin[22] |
| $^{47}$Ti FM | 32.50 | 0.00 | Baenziger[23] |
| $^{47}$Ti FM | 33.95 | 0.00 | Vlaic[48a] |

[a]The structure denoted "Vlaic" is the Baenziger structure of $TiCl_2$, but with $z = 0.23$ as suggested by Vlaic et al.[48] The AF supercell is as small as possible, containing two Ti with opposite moments.

Despite small differences in the structure, significantly different $C_Q$ parameters are found for the structures of Gal'perin and Baenziger. Vlaic et al.[48] have called for a re-evaluation of the crystal structure because their EXAFS measurements showed slightly shorter Ti−Cl bonds than the crystal structure suggests. The structures of both Gal'perin and Baenziger give the fractional coordinate of the chlorine position as $z = 0.25$, Vlaic suggests 0.23. In the calculations, this adapted structure has a significant effect on the chlorine $C_Q$, but the crystal symmetry is retained and consequently still a single chlorine site is expected. Alternative models in which the stacking of the layers is altered to follow the pattern in $MgCl_2$[47] or in which an AF ordering is considered have significantly less effect. Note that in the AF structure, the threefold symmetry disappears as is evidenced by a change in $\eta$. The Ti $C_Q$ is quite large and insensitive to the exact positions of the Cl, indicating that the higher coordination spheres cause the large EFG in these structures. An estimated $^{47}$Ti $C_Q$ of about 30 MHz gives NMR CT line widths in the range we observe in our experimental Ti spectrum. Again going to an AF structure appears not to affect the $C_Q$ much, but does substantially alter the local asymmetry $\eta$.

The results from $^{35,37}$Cl NMR do not conform to the reported crystal structure of $TiCl_2$. Nevertheless, powder XRD analysis of our samples is in quite good agreement with the literature (see the Supporting Information). To check if the divergent results of our experiments could be related to the sample integrity, a second sample of $TiCl_2$, originating from the same supplier, but with a different lot number, was analyzed and yielded exactly the same $^{47,49}$Ti and $^{35}$Cl NMR spectra. It is interesting to note that the calculated $^{35}$Cl quadrupolar parameters for the Gal'perin structure coincide nicely with the experimental parameters of the experimental $^{35}$Cl resonance observed at 94 ppm. Furthermore, the observed Ti line width does correspond to those expected from the calculated $C_Q$ values. Nevertheless, it becomes clear that either the crystal structure of $TiCl_2$ should be revised and/or the samples undergo (partial) degradation to a metastable/stable state, such as a different polymorph or a mixed oxide phase. Further research is needed to fully explain the solid-state NMR results in relation to the proposed XRD structures. In the present study, we direct our attention back to the ZNCs and leave a more in-depth investigation of the structures of $TiCl_2$ and its potential conversion products for a forthcoming study. We note that if the structure of active ZNCs resembles $TiCl_2$, it would be a relevant model system.

**Implications for ZNCs.** The $^{35}$Cl NMR spectra of the titanium chlorides that have been presented in the previous sections show strongly broadened quadrupolar line shapes, in particular for $TiCl_4$ and $TiCl_3$. In the neat titanium chlorides, these broad signals could be obtained relatively straightforwardly using variable offset echoes or QCPMG experiments. However, such broad lines will hamper the observation of the titanium-bound chlorines in ball-milled adducts and other ZNC samples. Preliminary calculations suggest $C_Q$ values of 14−19 MHz for the titanium-bound chlorines. These values are in line with the $C_Q$ values found for $TiCl_3$ and $TiCl_4$. This suggests that $^{35}$Cl NMR of ZNCs will be more challenging, particularly because we expect heterogeneity in the samples leading to a further distribution in NMR interaction parameters, meaning that line shapes will not be well defined. Most importantly, however, there will be strong "background" signals from $MgCl_2$.

Despite the uncertainties in the exact structure of $TiCl_2$, there is one interesting observation to make regarding the isotropic $^{35}$Cl chemical shifts for the titanium chlorides. Depending on the electronic state of the titanium, there is a strong dependency of the $^{35}$Cl shift, which varies from 875 ppm in $TiCl_4$ to 500 ppm in $TiCl_3$ and to 100−300 ppm in $TiCl_2$.

The $^{47,49}$Ti NMR spectrum of solid $TiCl_4$, with tetrahedrally coordinated Ti, showed relatively narrow, well-defined quadrupolar line shapes. Therefore, the spectrum was relatively easily obtained. In $TiCl_3$ and $TiCl_2$, Ti is octahedrally coordinated. These prove to have much larger $C_Q$ values, with the signal being unobservable for $TiCl_3$. The titanium sites in the ZNCs are expected to be octahedrally coordinated, and their environments are not likely to be very symmetric; consequently, very large line widths can be expected. This in combination with the much lower Ti concentration in the ZNCs may stand in the way of relevant Ti NMR analysis for catalyst samples particularly those with low titanium loading at natural abundance. Therefore, we require samples with highest possible loadings and signal enhancement schemes to have a chance for detecting signal from Ti in ZNC samples.

**$MgCl_2$/$TiCl_4$ Wet Impregnation.** As a first step toward the characterization of ZNCs, we prepared $MgCl_2$/$TiCl_4$ samples with a high titanium loading by wet impregnation of $MgCl_2$ with liquid $TiCl_4$, yielding samples MgTi1, MgTi2, and MgTi3 as described in the experimental section. In these samples, the amount of $TiCl_4$ has been varied to a different degree to see the effect on the line shape. When liquid $TiCl_4$ physisorbs onto the $MgCl_2$ surface, mobility reduces and hence resonances start to broaden, as shown by Ohashi et al.[8]

Figure S7A shows the $^{47,49}$Ti NMR spectra of MgTi1 and MgTi3 samples as well as neat liquid $TiCl_4$ for reference. The lines are clearly broadened with respect to liquid $TiCl_4$. The MgTi samples have a bicomponent line shape, which is particularly clear for the $^{47}$Ti resonance of $MgTi_3$. As shown in the Supporting Information, this bicomponent line shape results from a very small quadrupolar interaction giving rise to the appearance of the STs in the spectra. Figure S7B shows the $^{35}$Cl NMR spectra. Compared to liquid $TiCl_4$, we again observe a slight broadening of the resonance, but we do not yet see second-order quadrupolar line shape effects in this case.



DOI: 10.1021/acs.jpcc.9b02617
J. Phys. Chem. C 2019, 123, 14490−14500

A trend is observed in the spin-lattice relaxation times $T_1$ of the $^{47,49}$Ti nuclei along the sample series. The $T_1$ becomes significantly shorter in the MgTi samples compared to neat liquid $TiCl_4$ (see Table S2). On the basis of the sample preparation and the spectral appearance, we expect a higher amount of "coordinated" titanium going from MgTi to MgTi3. The faster relaxation in the latter sample results most likely from a slight increase in the asymmetry around the titanium nucleus. The quadrupolar interaction combined with local dynamics is an efficient relaxation mechanism.[49]

In these $MgCl_2/TiCl_4$ mixtures, we can straightforwardly detect $^{35}$Cl and $^{47,49}$Ti NMR signal. After wet impregnation, a slight broadening with respect to the neat $TiCl_4$ signal is observed, which is most likely the result of reduced mobility. We attribute this to immobilization of $TiCl_4$ on the surface. This association apparently does not change the coordination or oxidation state, as the positions of the resonances do not change, and we have not observed new signals from adsorbed Ti-species.

**$MgCl_2/TiCl_4$ Binary Adducts.** Ball-milled $MgCl_2/TiCl_4$ adducts are the most basic precatalyst systems. Usually, electron donors are added at this stage of catalyst preparation. To keep things as basic as possible and have high titanium loadings, we first investigate simple $MgCl_2/TiCl_4$ adducts, analogous to the experiments reported by Ohashi et al.[8] For co-milled $MgCl_2/TiCl_4$, they observed a shift of the titanium resonances and a broadening of the line widths as they increased the milling times, both of which are caused by an increasing quadrupolar interaction. Co-milling $MgCl_2$ and $TiCl_4$ generates nanosized particles with a few wt % $TiCl_4$. The sample characteristics are found in Table 4. Ball-milling not only generates high surfaces areas but also induces crystal defects. Therefore, ball-milling increases the number of $TiCl_4$ adsorption sites, which in turn increases the effectiveness of the catalyst. At the same time, this results in a more heterogeneous support and related distribution of $TiCl_4$ which complicates characterization.

**Table 4. Results from Elemental Analysis of Binary $MgCl_2/TiCl_4$ Adducts**

| samples code | Ti [wt %] | $TiCl_4$ [wt %] |
|---|---|---|
| 30 min | 0.84 | 3.03 |
| 2 h | 1.67 | 6.4 |
| 5 h | 3.11 | 12.3 |
| 8 h | 3.10 | 12.3 |
| 8 h washed | 3.03 | 12.0 |

We find a significant difference in titanium content between the samples, despite the lack of washing steps (i.e., free or uncoordinated $TiCl_4$ has not been washed away in the samples with short milling times). Longer ball-milling times apparently result in better binding of $TiCl_4$ to $MgCl_2$. Presumably, unbound $TiCl_4$ has evaporated from the samples. Only after 5 h of milling, the titanium content stabilizes. Washing of the 8 h milled sample does not lead to a significant lowering of the titanium content. The titanium content in our samples slightly exceeds the values reported by Ohashi et al. They have an increasing titanium content with longer milling times as well, but they performed washing steps for all their samples. We will evaluate the $^{35}$Cl and $^{47,49}$Ti NMR spectra of the binary adducts with shortest milling times because resonances are expected to be best accessible (i.e., narrowest) in these samples.

**$^{35}$Cl NMR of $MgCl_2/TiCl_4$ Adducts.** The detection of the titanium-bound chlorines in the preactive catalysts gives information about the molecular environment of the titanium site. The samples have a dominant $MgCl_2$ phase on which a minor amount of $TiCl_4$ is loaded. Despite a lower loading, the $^{35}$Cl NMR spectra of the two samples with shortest milling time have been acquired under both static and 15.625 kHz MAS conditions. Unlike the wet-impregnated samples, we find no signal from $TiCl_4$ around 865 ppm. This indicates that mobile $TiCl_4$ species are no longer present, in contrast to the results reported by Ohashi. At first glance, the spectra show only signal from the CT of the $MgCl_2$ phase.

To look more thoroughly for, potentially broadened, $TiCl_4$-derived sites, we performed variable offset (VOCS) experiments. Figure 6 shows that these spectra acquired over a frequency range of >1 MHz. Clearly, the signal is detected over a broad frequency range, and there is even some line shape to it. Around 0 kHz, the signal of the CT of bulk $MgCl_2$ is observed, which is very strong and vertically truncated in the figure. The remaining signal that is detected can be assigned to the STs of $MgCl_2$. Given the quadrupolar values of $C_Q$ = 4.6 MHz and $\eta$ = 0, the ST can be simulated as shown in the dotted trace. The intensity increase around ±1.1 MHz ($1/2 \times \omega_Q$) corresponds to the singularity of the ST. Also, the relative intensity of the signal is in agreement with the CT/ST-signal-ratio. Therefore, we can conclude that we do not observe additional $^{35}$Cl NMR signals from $TiCl_x$ in these samples.

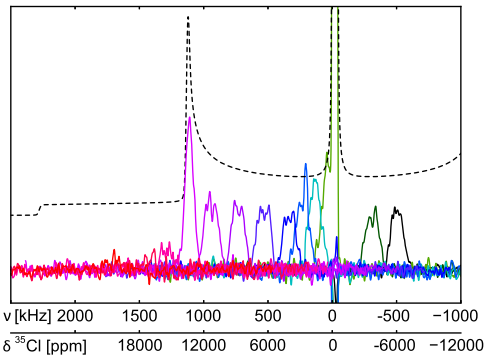


**Figure 6.** Static $^{35}$Cl NMR variable offset QCPMG (processed by summation of the echoes) spectra of 2 h ball-milled $MgCl_2/TiCl_4$ adduct. Transmitter offset steps between the spectra are usually 200 kHz, and 2048−4096 scans per offset are acquired, $B_0$ = 20.0 T. Dotted trace shows a simulation of the STs of $MgCl_2$.

In contrast to wet-impregnation, ball-milling has pronounced effects on the state of $TiCl_4$. Clearly, the coordination and/or oxidation state of $TiCl_4$ changes. The absence of the $TiCl_x$ signal in the $^{35}$Cl spectrum is most likely explained by a combination of the low intensity and the extremely large line width of these signals. On the basis of pulsed EPR correlation experiments (HYSCORE), Morra et al.[6] report $^{35}$Cl $C_Q$ values of ∼9 MHz for an activated ZNC, which would indeed give rise to strongly broadened resonances of a few hundred kHz that are beyond detection at low concentrations of a few percent.

**$^{47,49}$Ti NMR of $MgCl_2/TiCl_4$ Adducts.** From Table 4, it can be seen that the Ti-content in the samples ranges between 1 and 3%, which exceeds the loading measured by Ohashi et al.


DOI: 10.1021/acs.jpcc.9b02617
J. Phys. Chem. C 2019, 123, 14490−14500

Despite this, we were not able to reproduce their results. We succeeded in acquiring $^{47,49}$Ti signal using QCPMG experiments only after extensive signal averaging. The results are shown in Figure 7. After only 2 h of ball-milling, we observe a

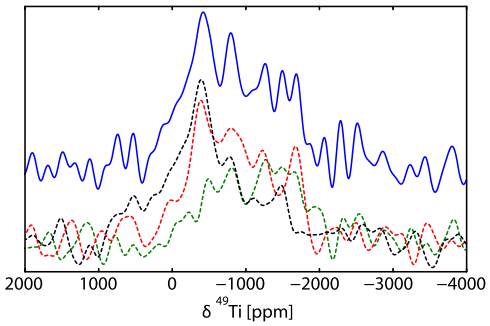


**Figure 7.** Static $^{47,49}$Ti QCPMG spectrum of 2 h ball-milled $MgCl_2$/$TiCl_4$ adduct (blue). The spectrum is the sum of three spectra obtained at different offsets (dashed lines) with approximately 80.000 scans per offset, where the transmitter is put at 0 ppm (black), −800 ppm (red), and −1400 ppm (green) to cover the full width of the resonance.

static line width of 110 kHz (overlapping signal of both $^{47}$Ti and $^{49}$Ti). The obtained spectrum is much broader compared to the results reported by Ohashi et al., who had a $^{49}$Ti resonance spanning only 5 kHz (at 15 kHz MAS and 21.8 T) for a sample that was ball-milled for 20 h.

In order to properly determine the width of the resonance, spectra have been recorded at various resonance offsets, compare the black and green dashed lines. Although there is a bit more intensity at the right-hand side of the green spectrum compared to the black one, they span almost the same frequency range. The large line width points to a large quadrupole interaction of the adsorbed titanium sites. This indicates that a strong reduction of the local symmetry around the titanium nucleus has occurred compared to $TiCl_4$ and the wet-impregnated samples. The observed line is substantially narrower, however, than that observed for $TiCl_2$. Because of the limited S/N-ratio in the presented spectrum, the exact line shape cannot be determined by fitting. However, it appears that the line shape is not completely featureless and a peak maximum is observed around −400 ppm. Compared to solid $TiCl_4$, the isotropic chemical shift(s) appear(s) to be at a significantly lower shift value. In agreement with the chlorine data, we observe a pronounced effect of ball-milling on the spectra of $TiCl_x$, which indicates a change in the coordination and/or the conformation of Ti upon binding to $MgCl_2$.

In order to understand this better, we carried out DFT calculations for several structures modeling $TiCl_4$ on $MgCl_2$ surfaces (details can be found in Supporting Information Section S6). These are "4-110" [four-coordinated Ti as mononuclear $TiCl_4$ on the edge of a $MgCl_2$ ribbon representing $MgCl_2$ (110)], "5-104" [five-coordinated Ti, mononuclear, (104)], "6-110" [six-coordinated Ti, mononuclear, (110), the "Corradini site"], and "6-104" [six-coordinated Ti, dinuclear, (104)]. The labeling of the structures is according to ref 50. In our calculations, the four-coordination on the 110 surface was not stable and relaxed to 6-104. The calculated NMR parameters are summarized in Table 5. The calculated $^{47}$Ti $C_Q$ values of all sites are of the order of 12−16 MHz which will give line widths of the order 100 kHz, in line with our experimental

**Table 5. Summary of PBE-DFT Calculations on Models of $TiCl_4$ Units on Edges of $MgCl_2$ Slabs**[a]

| | $C_Q$ [MHz] | $\sigma_{iso}$ [ppm] |
|---|---|---|
| 5-104 | 15.6 | −981 |
| 6-110 | 11.6 | −875 |
| 6-104 | 12.5 | −872 |

[a]The $C_Q$ (absolute values) is for $^{47}$Ti. Shieldings are absolute (not referenced).

observations. Unfortunately, the differences in calculated $C_Q$ are too small to favor specific sites based on the observed line widths. The calculated isotropic shieldings do show a distinct difference between the five-coordinated and six-coordinated Ti with the latter being nearly independent of the surface to which the $TiCl_4$ binds. The five-coordinated site has an isotropic shielding similar to that calculated for four-coordinated Ti in $TiCl_4$ (−977 ppm, Table S1). The six-coordinated sites are more shielded by approximately 100 ppm. This is smaller than what we observe experimentally but in the same direction. Indeed, the same mononuclear and binuclear binding modes were observed to lead to preferred octahedral six-coordination in a recent theoretical study on $(MgCl_2)_n(TiCl_4)_m$ clusters.[7] Another recent theoretical study, also using clusters, reports the same three structural motifs as in Table 5.[51] These authors find a substantial fraction of mononuclear 5-104 ("mononuclear {100}" in their study), but that is outweighed by a much larger fraction of 6-110, that is, six-coordinated Ti.

**$^{47,49}$Ti NMR of ZNC.** Following the successful acquisition of Ti signal for the 2 h milled $MgCl_2$/$TiCl_4$ adduct, we used the same experiment for two systems with a more complex composition: industrial precatalyst CAT4 and a cocatalyst containing sample TMC-M. The primary questions are whether significant changes in the line shape can be seen and whether the titanium visibility changes.

The industrial precatalyst CAT4 consists of $MgCl_2$, $TiCl_4$, and the electron donor di-*n*-butylphthalate (DnBP). The titanium content of this sample is ∼2 wt % and thus slightly higher than the 2 h ball-milled sample. If the donor coordinates in the vicinity of Ti, this might have an effect on the quadrupole interaction leading to a change in the line shape.

Sample TMC-M is an adduct of $MgCl_2$ and $TiCl_4$ that has been treated with an excess of trimethylaluminum (TMA). It contains ∼3.5 wt % Ti, and it was shown that a fraction of Ti is reduced to EPR-visible $Ti^{3+}$.[11] This paramagnetic species is most likely not detectable by NMR. Potential other EPR silent $Ti^{3+}$ (dimeric, polymeric species with exchange interactions) and $Ti^{2+}$ states that might or might not be observable, could be present as well, but this should become clear from the spectral intensity. Again, line shape changes might occur as well if the cocatalyst binds near the titanium.

The resulting Ti spectra are shown in Figure 8. In contrast to the 2 h ball-milled sample, the spectra for CAT4 and TMC-M are recorded at a single transmitter offset put at −400 ppm, explaining why they have a bit less intensity on the right-hand side of the resonance. All spectra are scaled according to the titanium content of the samples as well as the number of scans. This allows a semiquantitative comparison of spectra. CAT4 and the 2 h milled adduct give very comparable spectra, both in terms of signal intensity and line shape. This shows that the titanium environment is not significantly altered by the presence of the donor, which implies that it does not bind


DOI: 10.1021/acs.jpcc.9b02617
J. Phys. Chem. C 2019, 123, 14490−14500

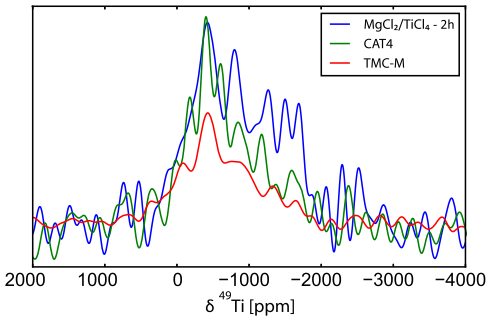


**Figure 8.** Static $^{47,49}$Ti QCPMG spectra of 2 h ball-milled $MgCl_2$/$TiCl_4$ adduct (blue, see Figure 7), CAT4 (green, about 250.000 scans), and TMC-M (red, about 400.0000 scans).

directly to titanium or in its close proximity. Even with the low S/N-ratio, it is clear that TMC-M gives significantly less signal than the other two samples. This confirms the partial reduction of Ti to NMR undetectable $Ti^{3+}$ species. However, the line shape of the remaining signal appears similar to the spectra of the other samples, indicating that a large fraction of the supported Ti-sites is unaffected by the cocatalyst. Clearly, the presence of both donor and cocatalyst does not have a significant effect on the local titanium environment of the NMR visible titanium sites, as the line shape and width appear very comparable in all samples. Unfortunately, for those sites that are reduced, we cannot obtain an NMR signal. The local environment of these sites may well be altered. EPR spectroscopy probes the local environment of isolated $Ti^{3+}$ sites. Morra et al.[6] showed hyperfine coupling to nearby $^{27}$Al nuclei in an activated catalyst using a HYSCORE experiment. In a previous $^{27}$Al NMR study of these systems,[11] we observed a very high reactivity of the aluminum alkyls with the surface in all samples, leading to a multitude of aluminum coordinations. This indicates why only a fraction of the titanium in the catalyst system is converted into active $Ti^{3+}$ species. Our current Ti NMR observations corroborate that finding.

## CONCLUSIONS

In this contribution, we presented a $^{35,37}$Cl and $^{47,49}$Ti NMR study of titanium chlorides as model compounds for the active site in ZNCs. Static $^{35}$Cl spectra from solid $TiCl_4$ and $TiCl_3$ show that these materials are characterized by large $C_Q$'s (12−14 MHz). Our DFT calculations of both EFG and CSA parameters are in excellent agreement with experimental values. For $TiCl_2$, we find smaller quadrupolar coupling parameters, although we are not certain about the actual structure of the $TiCl_2$ samples that were studied. The titanium chlorides show $^{35}$Cl NMR properties that call for dedicated experiments and imply challenges for the extension toward the characterization of real catalyst samples. The significant "background" signal from $MgCl_2$, both the CT and the ST, makes the observation of broad signal from Ti−Cl sites in ZNCs even more challenging.

Titanium chlorides have different coordination environments for titanium (tetrahedral, octahedral). For solid $TiCl_4$, with titanium tetrahedrally coordinated by chlorine, there is a small quadrupolar interaction because the tetrahedron is not fully symmetric. This shows the sensitivity of the Ti-nucleus for the local environment. Unfortunately, no Ti NMR spectrum could be obtained for $TiCl_3$, but DFT calculations predict it to have an extremely large $C_Q$. Also, for $TiCl_2$, a substantial $C_Q$ was calculated. In this case, we were able to acquire an extremely broad resonance, corresponding to the calculated $C_Q$-value.

The Ti NMR signal in the ZNCs could only be observed after extensive signal averaging and was broad compared to the reported literature. The results shown in the literature suggest only an immobilization of $TiCl_4$ on the surface upon ball-milling. We observe such effects only upon wet impregnation of $MgCl_2$ with $TiCl_4$. The absence of additional narrow Cl resonances and the broad Ti signal in ball-milled samples indicates a strong binding to the support's surface with a change in coordination and/or a significantly different conformation compared to physisorbed $TiCl_4$. DFT calculations generate $C_Q$ values for the proposed surface sites that match experimental observation, whereas chemical shift values point to a higher shielding for the octahedral sites, albeit smaller than observed. The overall appearance of the Ti signal was found not to change significantly between samples with different compositions; both the DnBP electron donor and the TMA cocalyst do not appear to have a direct interaction with the NMR observable titanium site. However, the addition of the Al-alkyl results in signal loss as the consequence of reduction of a fraction of the Ti-site. This proves that the active $Ti^{3+}$ sites in the catalyst derive from the pool of Ti-sites observed in the precatalysts. As a result of the high reactivity of the aluminum-alkyl, reacting with many different surface species, only a small fraction of the surface bound Ti-species is activated.

## ASSOCIATED CONTENT

### Supporting Information

The Supporting Information is available free of charge on the ACS Publications website at DOI: 10.1021/acs.jpcc.9b02617.

Additional information on sample preparation, $^{35,37}$Cl and $^{47,49}$Ti NMR spectra, calculations and powder XRD pattern of $TiCl_2$ (PDF)

## AUTHOR INFORMATION

### Corresponding Author

*E-mail: a.kentgens@nmr.ru.nl.

### ORCID

E. S. (Merijn) Blaakmeer: 0000-0001-5108-5655
Gilles A. de Wijs: 0000-0002-1818-0738
Arno P. M. Kentgens: 0000-0001-5893-4488

### Notes

The authors declare no competing financial interest.

## ACKNOWLEDGMENTS

The authors acknowledge the technical support with the SSNMR measurements provided by Gerrit Janssen and Hans Janssen, dr. P. Tinnemans from Radboud University for powder XRD measurements and are grateful to SABIC for providing the precatalyst sample. Prof. V. Busico and G. Antinucci from the University of Naples are acknowledged for providing the ball-milled adducts and the TMC-M sample. Support of the Dutch Organization for scientific research NWO for the "Solid state NMR facility for advanced materials science" in Nijmegen is gratefully acknowledged.



DOI: 10.1021/acs.jpcc.9b02617
J. Phys. Chem. C 2019, 123, 14490−14500

## REFERENCES


(1) *Polypropylene Handbook: Polymerization, Characterization, Properties, Processing, Applications*; Moore, E. P., Jr., Ed.; Hanser Publishers: Munich, Germany, 1996.

(2) Credendino, R.; Liguori, D.; Fan, Z.; Morini, G.; Cavallo, L. Toward a Unified Model Explaining Heterogeneous Ziegler-Natta Catalysis. *ACS Catal.* **2015**, *5*, 5431−5435.

(3) Brambilla, L.; Zerbi, G.; Piemontesi, F.; Nascetti, S.; Morini, G. Structure of $MgCl_2$-$TiCl_4$ Complex in Co-Milled Ziegler-Natta Catalyst Precursors with Different $TiCl_4$ Content: Experimental and Theoretical Vibrational Spectra. *J. Mol. Catal. A: Chem.* **2007**, *263*, 103−111.

(4) D'Amore, M.; Credendino, R.; Budzelaar, P. H.; Causà, M.; Busico, V. A Periodic Hybrid DFT Approach (Including Dispersion) to $MgCl_2$-Supported Ziegler-Natta catalysts - 1: $TiCl_4$ Adsorption on $MgCl_2$ Crystal Surfaces. *J. Catal.* **2012**, *286*, 103−110.

(5) D'Amore, M.; Thushara, K. S.; Piovano, A.; Causà, M.; Bordiga, S.; Groppo, E. Surface Investigation and Morphological Analysis of Structurally Disordered $MgCl_2$ and $MgCl_2$/$TiCl_4$ Ziegler-Natta Catalysts. *ACS Catal.* **2016**, *6*, 5786−5796.

(6) Morra, E.; Giamello, E.; Van Doorslaer, S.; Antinucci, G.; D'Amore, M.; Busico, V.; Chiesa, M. Probing the Coordinative Unsaturation and Local Environment of $Ti^{3+}$ Sites in an Activated High-Yield Ziegler-Natta Catalyst. *Angew. Chem., Int. Ed.* **2015**, *54*, 4857−4860.

(7) Zorve, P.; Linnolahti, M. Adsorption of Titanium Tetrachloride on Magnesium Dichloride Clusters. *ACS Omega* **2018**, *3*, 9921−9928.

(8) Ohashi, R.; Saito, M.; Fujita, T.; Nakai, T.; Utsumi, H.; Deguchi, K.; Tansho, M.; Shimizu, T. Observation of $^{47,49}$Ti NMR Spectra of $TiCl_4$/$MgCl_2$-Catalysts under an Ultrahigh Magnetic Field. *Chem. Lett.* **2012**, *41*, 1563−1565.

(9) Rossini, A. J.; Hung, I.; Schurko, R. W. Solid-State $^{47/49}$Ti NMR of Titanocene Chlorides. *J. Phys. Chem. Lett.* **2010**, *1*, 2989−2998.

(10) Blaakmeer, E. S.; Antinucci, G.; Busico, V.; van Eck, E. R. H.; Kentgens, A. P. M. Solid-State NMR Investigations of $MgCl_2$ Catalyst Support. *J. Phys. Chem. C* **2016**, *120*, 6063−6074.

(11) Blaakmeer, E. S.; van Eck, E. R. H.; Kentgens, A. P. M. The Coordinative State of Aluminium Alkyls in Ziegler-Natta Catalysts. *Phys. Chem. Chem. Phys.* **2018**, *20*, 7974−7988.

(12) Larsen, F. H.; Jakobsen, H. J.; Ellis, P. D.; Nielsen, N. C. Sensitivity-Enhanced Quadrupolar-Echo NMR of Half-Integer Quadrupolar Nuclei. Magnitudes and Relative Orientation of Chemical Shielding and Quadrupolar Coupling Tensors. *J. Phys. Chem. A* **1997**, *101*, 8597−8606.

(13) Kresse, G.; Hafner, J. Ab Initio Molecular Dynamics for Liquid Metals. *Phys. Rev. B: Condens. Matter Mater. Phys.* **1993**, *47*, 558−561.

(14) Kresse, G.; Furthmüller, J. Efficient Iterative Schemes for Ab Initio Total-Energy Calculations using a Plane-Wave Basis Set. *Phys. Rev. B: Condens. Matter Mater. Phys.* **1996**, *54*, 11169−11186.

(15) Blöchl, P. E. Projector Augmented-Wave Method. *Phys. Rev. B: Condens. Matter Mater. Phys.* **1994**, *50*, 17953−17979.

(16) Kresse, G.; Joubert, D. From Ultrasoft Pseudopotentials to the Projector Augmented-Wave Method. *Phys. Rev. B: Condens. Matter Mater. Phys.* **1999**, *59*, 1758−1775.

(17) Perdew, J. P.; Burke, K.; Ernzerhof, M. Generalized Gradient Approximation Made Simple. *Phys. Rev. Lett.* **1996**, *77*, 3865−3868.

(18) Perdew, J. P.; Burke, K.; Ernzerhof, M. Generalized Gradient Approximation Made Simple [Phys. Rev. Lett. 77, 3865 (1996)]. *Phys. Rev. Lett.* **1997**, *78*, 1396.

(19) Krukau, A. V.; Vydrov, O. A.; Izmaylov, A. F.; Scuseria, G. E. Influence of the Exchange Screening Parameter on the Performance of Screened Hybrid Functionals. *J. Chem. Phys.* **2006**, *125*, 224106.

(20) Dawson, A.; Parkin, A.; Parsons, S.; Pulham, C. R.; Young, A. L. C. Titanium(IV) Chloride at 150K. *Acta Crystallogr., Sect. E: Struct. Rep. Online* **2002**, *58*, i95−i97.

(21) Troyanov, S. I.; Snigireva, E. M.; Rybakov, V. X-ray Diffraction Study of Phase Transition in $\alpha$-$TiCl_3$. *Zh. Neorg. Khim.* **1991**, *36*, 1117−1122.

(22) Gal'perin, E.; Sandler, R. Crystal Structure of $TiCl_2$. *Sov. Phys. Crystallogr.* **1962**, *7*, 217−219.

(23) Baenziger, N. C.; Rundle, R. E. The structure of TiCl2. *Acta Crystallogr.* **1948**, *1*, 274.

(24) Pickard, C. J.; Mauri, F. All-Electron Magnetic Response with Pseudopotentials: NMR Chemical Shifts. *Phys. Rev. B: Condens. Matter Mater. Phys.* **2001**, *63*, 245101.

(25) Yates, J. R.; Pickard, C. J.; Mauri, F. Calculation of NMR Chemical Shifts for Extended Systems using Ultrasoft Pseudopotentials. *Phys. Rev. B: Condens. Matter Mater. Phys.* **2007**, *76*, 024401.

(26) de Wijs, G. A.; Laskowski, R.; Blaha, P.; Havenith, R. W. A.; Kresse, G.; Marsman, M. NMR Shieldings from Density Functional Perturbation Theory: GIPAW Versus All-Electron Calculations. *J. Chem. Phys.* **2017**, *146*, 064115.

(27) Petrilli, H. M.; Blöchl, P. E.; Blaha, P.; Schwarz, K. Electric-Field-Gradient Calculations using the Projector Augmented Wave Method. *Phys. Rev. B: Condens. Matter Mater. Phys.* **1998**, *57*, 14690−14697.

(28) King-Smith, R. D.; Payne, M. C.; Lin, J. S. Real-Space Implementation of Nonlocal Pseudopotentials for First-Principles Total-Energy Calculations. *Phys. Rev. B: Condens. Matter Mater. Phys.* **1991**, *44*, 13063−13066.

(29) Chapman, R. P.; Widdifield, C. M.; Bryce, D. L. Solid-State NMR of Quadrupolar Halogen Nuclei. *Prog. Nucl. Magn. Reson. Spectrosc.* **2009**, *55*, 215−237.

(30) Skibsted, J.; Jakobsen, H. J. $^{35}$Cl and $^{37}$Cl Magic-Angle Spinning NMR Spectroscopy in the Characterization of Inorganic Perchlorates. *Inorg. Chem.* **1999**, *38*, 1806−1813.

(31) Rossini, A. J.; Mills, R. W.; Briscoe, G. A.; Norton, E. L.; Geier, S. J.; Hung, I.; Zheng, S.; Autschbach, J.; Schurko, R. W. Solid-State Chlorine NMR of Group IV Transition Metal Organometallic Complexes. *J. Am. Chem. Soc.* **2009**, *131*, 3317−3330.

(32) Dehmelt, H. G. Nuclear Quadrupole Resonance in Some Metal Chlorides and Oxychlorides. *J. Chem. Phys.* **1953**, *21*, 380.

(33) Hamlen, R. P.; Koski, W. S. $^{35}$Cl Nuclear Quadrupole Resonances in $TiCl_4$ and $WCl_6$. *J. Chem. Phys.* **1956**, *25*, 360.

(34) Reddoch, A. H. Nuclear Quadrupole Resonance in $TiCl_4$, $ThCl_4$, $NbCl_5$, and $TaCl_5$. *J. Chem. Phys.* **1961**, *35*, 1085−1089.

(35) Sparks, S. W.; Ellis, P. D. Platinum-195 Shielding Tensors in Potassium Hexachloroplatinate(IV) and Potassium Tetrachloroplatinate(II). *J. Am. Chem. Soc.* **1986**, *108*, 3215−3218.

(36) Massiot, D.; Farnan, I.; Gautier, N.; Trumeau, D.; Trokiner, A.; Coutures, J. P. $^{71}$Ga and $^{69}$Ga Nuclear Magnetic Resonance Study of $\beta$-$Ga_2O_3$: Resolution of Four- and Six-Fold Coordinated Ga Sites in Static Conditions. *Solid State Nucl. Magn. Reson.* **1995**, *4*, 241−248.

(37) Bak, M.; Rasmussen, J. T.; Nielsen, N. C. SIMPSON: A General Simulation Program for Solid-State NMR Spectroscopy. *J. Magn. Reson.* **2000**, *147*, 296−330.

(38) Bryce, D. L.; Bultz, E. B. Alkaline Earth Chloride Hydrates: Chlorine Quadrupolar and Chemical Shift Tensors by Solid-State NMR Spectroscopy and Plane Wave Pseudopotential Calculations. *Chem.—Eur. J.* **2007**, *13*, 4786−4796.

(39) Bryce, D. L.; Sward, G. D. Chlorine-35/37 NMR Spectroscopy of Solid Amino Acid Hydrochlorides: A Refinement of Hydrogen-Bonded Proton Positions Using Experiment and Theory. *J. Phys. Chem. B* **2006**, *110*, 26461−26470.

(40) Bryce, D. L.; Sward, G. D.; Adiga, S. Solid-State $^{35/37}$Cl NMR Spectroscopy of Hydrochloride Salts of Amino Acids Implicated in Chloride Ion Transport Channel Selectivity: Opportunities at 900 MHz. *J. Am. Chem. Soc.* **2006**, *128*, 2121−2134.

(41) van Meerten, S. G. J.; Franssen, W. M. J.; Kentgens, A. P. M. ssNake: A cross-platform open-source NMR data processing and fitting application. *J. Magn. Reson.* **2019**, *301*, 56−66.

(42) Natta, G.; Corradini, P.; Allegra, G. The Different Crystalline Modifications of $TiCl_3$, a Catalyst Component for the Polymerization of $\alpha$-olefins. I: $\alpha$-, $\beta$-, $\gamma$-$TiCl_3$. II: $\delta$-TiCl3. *J. Polym. Sci.* **1961**, *51*, 399−410.




DOI: 10.1021/acs.jpcc.9b02617
J. Phys. Chem. C 2019, 123, 14490−14500

(43) Barnes, R. G.; Segel, S. L. Pure Nuclear Quadrupole Resonances in Paramagnetic Iron-Group Halides. *Phys. Rev. Lett.* **1959**, *3*, 462−464.
(44) Cavallone, F.; Pollini, I.; Spinolo, G. Electrical Properties of $\alpha$-$TiCl_3$ Crystals. *Lett. Nuovo Cimento* **1970**, *4*, 764−766.
(45) Maurelli, S.; Morra, E.; Van Doorslaer, S.; Busico, V.; Chiesa, M. EPR Investigation of $TiCl_3$ Dissolved in Polar Solvents − Implications for the Understanding of Active Ti(III) Species in Heterogeneous Ziegler−Natta Catalysts. *Phys. Chem. Chem. Phys.* **2014**, *16*, 19625−19633.
(46) Holleman, A.; Wiberg, E.; Wiberg, N. *Inorganic Chemistry*; Academic Press: San Diego, 2001; Chapter 25, p 1335.
(47) Partin, D. E.; O'Keeffe, M. The Structures and Crystal Chemistry of Magnesium Chloride and Cadmium Chloride. *J. Solid State Chem.* **1991**, *95*, 176−183.
(48) Vlaic, G.; Bart, J. C. J.; Cavigiolo, W.; Mobilio, S.; Navarra, G. EXAFS Structural Parameters for some Titanium Halides. *Chem. Phys.* **1982**, *64*, 115−122.
(49) Johnson, K. J.; Hunt, J. P.; Dodgen, H. W. Chlorine-35 NMR Study of the Shifts and Line Shapes of Some Liquid Inorganic Chlorides. *J. Chem. Phys.* **1969**, *51*, 4493−4496.
(50) Linnolahti, M.; Pakkanen, T. A.; Bazhenov, A. S.; Denifl, P.; Leinonen, T.; Pakkanen, A. Alkylation of titanium tetrachloride on magnesium dichloride in the presence of Lewis bases. *J. Catal.* **2017**, *353*, 89−98.
(51) Takasao, G.; Wada, T.; Thakur, A.; Chammingkwan, P.; Terano, M.; Taniike, T. Machine Learning-Aided Structure Determination for $TiCl_4$-Capped $MgCl_2$ Nanoplate of Heterogeneous Ziegler-Natta Catalyst. *ACS Catal.* **2019**, *9*, 2599−2609.



DOI: 10.1021/acs.jpcc.9b02617
*J. Phys. Chem. C* 2019, 123, 14490−14500